let-7 miRNA controls CED-7 homotypic adhesion and EFF-1–mediated axonal self-fusion to restore touch sensation following injury

Atrayee Basu[a], Shirshendu Dey[b], Dharmendra Puri[a], Nilanjana Das Saha[a], Vidur Sabharwal[c], Pankajam Thyagarajan[a], Prerna Srivastava[a], Sandhya Padmanabhan Koushika[c], and Anindya Ghosh-Roy[a,d,1]

[a]National Brain Research Centre, Manesar, Nainwal Mode, Gurgaon, Haryana 122051, India; [b]Bruker India Scientific Private Ltd, New Delhi 110019, India; [c]Department of Biological Sciences, Tata Institute of Fundamental Research, Mumbai 400 005, India; and [d]Wellcome Trust–Department of Biotechnology India Alliance, Banjara Hills, Hyderabad, Telangana 500034, India

Edited by Martin Chalfie, Columbia University, New York, NY, and approved October 11, 2017 (received for review March 21, 2017)

Neuronal injury often leads to devastating consequences such as loss of senses or locomotion. Restoration of function after injury relies on whether the injured axons can find their target cells. Although fusion between injured proximal axon and distal fragment has been observed in many organisms, its functional significance is not clear. Here, using *Caenorhabditis elegans* mechanosensory neurons, we address this question. Using two femtosecond lasers simultaneously, we could scan and sever posterior lateral microtubule neurons [posterior lateral microtubules (PLMs)] on both sides of the worm. We showed that axotomy of both PLMs leads to a dramatic loss of posterior touch sensation. During the regenerative phase, only axons that fuse to their distal counterparts contribute to functional recovery. Loss of *let-7* miRNA promotes functional restoration in both larval and adult stages. In the L4 stage, loss of *let-7* increases fusion events by increasing the mRNA level of one of the cell-recognition molecules, CED-7. The ability to establish cytoplasmic continuity between the proximal and distal ends declines with age. Loss of *let-7* overcomes this barrier by promoting axonal transport and enrichment of the EFF-1 fusogen at the growing tip of cut processes. Our data reveal the functional property of a regenerating neuron.

femtosecond laser | axotomy | gentle touch | fusion | let-7

Accidental damage of neuronal processes often causes functional losses that affect locomotion, sensation, and many other higher brain functions (1, 2). Functional recovery in the adult nervous system is limited, since the injured nerves fail to find their postsynaptic partners while regrowing (1). After axotomy, the distal axon undergoes a degenerative process named "Wallerian degeneration" (3). In many organisms, such as *Aplysia*, crayfish, leeches, and worms, injured processes can reconnect with their severed distal processes (4–9). This phenomenon, "axonal fusion" (4–9), prevents the degeneration of the severed distal axon. Evidence suggests that axonal fusion suppresses the electrophysiological changes caused by injury (8). Based on these observations, it is logical to postulate that axonal fusion would lead to functional repair. However, quantitative behavioral evidence toward this is lacking.

Caenorhabditis elegans is a useful model for studying axon regrowth after injury (10). Genetic screens have identified a large number of pathways specifically required for adult axon regrowth (11, 12). The mechanosensory neurons responsible for gentle touch sensation are often used for studying axonal response to laser injury (10, 13). After laser axotomy of a posterior touch neuron (posterior lateral microtubule, PLM), a considerable number of axons become fused to their distal counterparts (9, 14). This phenomenon is dependent on the fusogen molecule EFF-1 and cell-recognition pathways (9, 15). Although, functional regeneration in a D-type GABAergic motor neuron was reported earlier (16), no study to date has addressed the functional aspect of regeneration in touch neurons. One constraint in studying the behavioral consequences of axotomy is that the severing of multiple neurons is often required to observe the effect of injury on behavior. Touch neurons are located laterally on both the sides of the worm body (17). Using conventional illumination methods, it is challenging to simultaneously visualize and cut the PLM axon that is located on the bottom side (16, 18).

We overcame this limitation by using the 3D sectioning capability of a two-photon microscope (19). By employing two independent laser beams, one femtosecond laser to localize axons and the other to sever them, we could systematically analyze the effect on gentle touch sensation when one PLM is axotomized versus when two PLMs are axotomized. Cutting both PLMs strongly reduces the posterior touch response. During the regenerative growth phase, we find that only the axons that successfully fuse with their distal counterparts contribute to functional recovery. Axonal fusion is also correlated with the restoration of axonal transport at the distal fragment. We further showed that *let*-7 miRNA inhibits the establishment of cytoplasmic continuity in a cell-autonomous manner during late larval and adult stages. Loss of *let-7* increases the level of *ced-7* mRNA, and the probability of a fusion event is increased in late larval stage. As the worm ages, the axonal transport is perturbed, and a key fusogen molecule, EFF-1, becomes limiting at the growing tips of cut axon. Loss of *let-7* overcomes these barriers by delaying neuronal aging and stimulating functional recovery.

Significance

In many organisms axonal fragments can rejoin by self-fusion after neuronal injury. It is hypothesized that cell fusion would be an efficient way to repair functional loss after injury. In this study, we tested this hypothesis using the *Caenorhabditis elegans* sensory neurons that are responsible for gentle touch sensation. We found that fusion between the proximal and distal fragments of an injured posterior touch neuron (the posterior lateral microtubule) promotes functional recovery in an age-dependent manner. We also discovered that *let-7* miRNA inhibits functional restoration via EFF-1–mediated axonal self-fusion by reducing *ced-7* expression. Our work established that the axon fusion process has functional significance in the maintenance of neuronal integrity throughout the life span of an organism.

Author contributions: A.B., S.D., P.T., S.P.K., and A.G.-R. designed research; A.B., D.P., N.D.S., V.S., and P.T. performed research; A.B., S.D., D.P., P.T., and P.S. contributed new reagents/analytic tools; A.B., D.P., N.D.S., V.S., and A.G.-R. analyzed data; and A.B., S.D., S.P.K., and A.G.-R. wrote the paper.

The authors declare no conflict of interest.

This article is a PNAS Direct Submission.

[1]To whom correspondence should be addressed. Email: anindya@nbrc.ac.in.

This article contains supporting information online at www.pnas.org/lookup/suppl/doi:10.1073/pnas.1704372114/-/DCSupplemental.

Results

Axotomy of PLM Neurons on both Sides Perturbs Posterior Touch Sensation. Gentle touch sensation on either the anterior or posterior end of a worm involves three neurons, two of which are located bilaterally just beneath the cuticle (Fig. 1*A*) (17). Using imaging techniques such as widefield or confocal microscopy and a single femtosecond laser, researchers to date have axotomized only one PLM neuron located on either the left or the right side (18, 20–23). Due to this limitation, researchers also had note the side of axotomy and subsequently track the worms during further analysis (9, 11, 20). The neuron on the other side can be illuminated using two-photon microscopy (19). Here, we simultaneously used the two femtosecond lasers of a two-photon microscope, one at 920 nm for imaging GFP and the other at 720 nm for cutting, controlled independently by two galvanometer-based laser scanners (Fig. 1*A* and Fig. S1*A*), and cut PLM neurons on both sides (Fig. 1*B*, Fig. S1*B*, and Movie S1).

A worm that is moving forward responds to a gentle touch in the anterior side by reversing, and a worm that is moving backwards likewise responds to a posterior touch by reversing (Movie S2). Using this assay, one can measure touch sensation with a posterior touch response index (PTRI) (24). Since the worms were subjected to axotomy under anesthetized conditions (9, 11, 20), the earliest behavioral test was conducted 10 h after axotomy. Cutting the PLM neuron on one side 50 μm away from the cell body (Fig. 1 *A* and *B*) reduces the PTRI at the experimental side significantly, from 0.95 ± 0.01 (mean ± SEM) to 0.62 ± 0.009 (***$P < 0.0001$; Newman–Keuls multiple comparisons test) (Fig. 1*C*). A mild but significant reduction was also noticed in the control side compared with laser-treated control worms, which were subjected to a laser pulse 6 μm away from the axon in the dorso–ventral axis. However, the anterior touch response index (ATRI) for both sides remained unaffected (Fig. 1*C*). A loss in PTRI on the control side indicates that the PLM neurons on both sides coordinate to sense the gentle touch. This is further strengthened by the observation that cutting PLMs on both sides produces a synergistic reduction in PTRI from 0.62 ± 0.009 to 0.51 ± 0.005 (***$P < 0.0001$; Newman–Keuls multiple comparisons test) (Fig. 1*C* and Movie S3). To rule out the effect of anesthesia in this phenomenon, we repeated the experiment by immobilizing the worms using beads (25, 26). This method also showed that cutting two PLMs gives a stronger effect than cutting one PLM (***$P < 0.0001$; Newman–Keuls multiple comparisons test) (Fig. S1*C*). This phenomenon was reproduced in other transgenic strains, namely *zdIs5* (P*mec-4*-GFP) and *tbIs222* (P*mec-4*-mCherry) (Fig. S1 *D* and *E*). A similar trend was also noticed on cutting anterior touch neurons (anterior lateral microtubules, ALMs) on both sides (*$P < 0.0001$; Newman–Keuls multiple comparisons test) (Fig. S1*F*). To evaluate the activity of a single PLM, we ablated one PLM and one posterior ventral microtubule (PVM) at the L2 stage before axotomizing the intact PLM at the L4 stage. We found that the side with the intact PLM before axotomy gave a PTRI value of 0.72 ± 0.012, which dropped to 0.50 ± 0.012 (***$P < 0.0001$; Newman–Keuls multiple comparisons test) after cutting (Fig. 1*D*). This value is similar to the PTRI value in a given side after two-side axotomy. This indicated that our two-sided-axotomy paradigm is similar to evaluating the activity from a single PLM.

We asked, how the PTRI remained at 50% even after two axons had been cut. A previous study on touch neurons indicated that synaptic branches have a functional significance in touch sensation (27). We noticed that cutting only the branches abolished

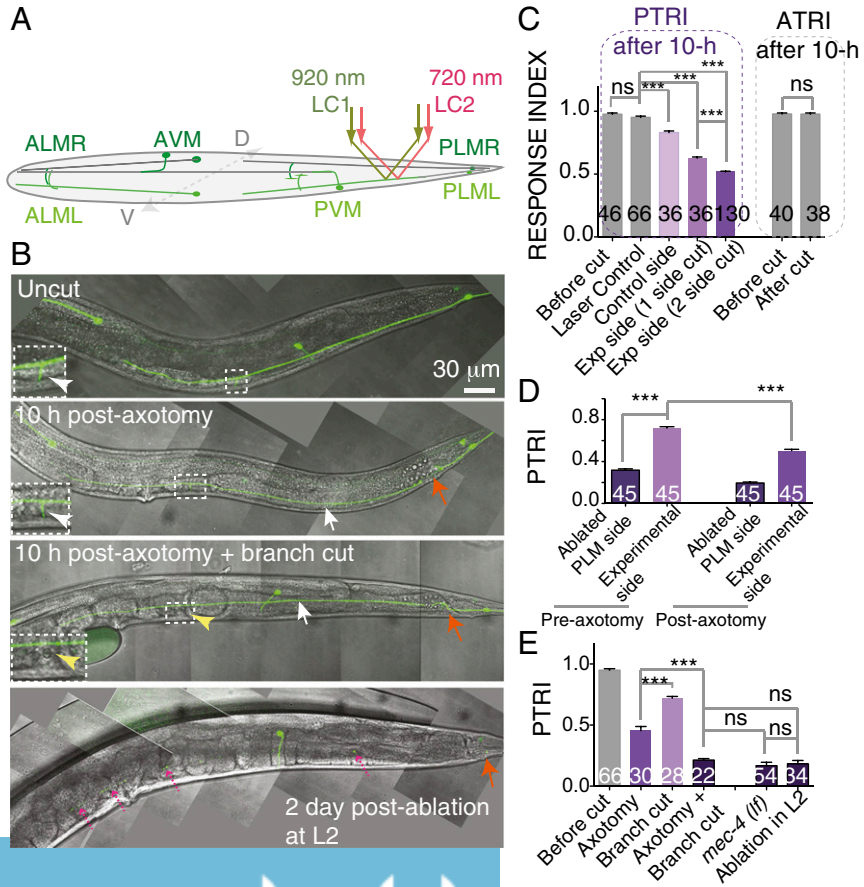

Fig. 1. Effect of axotomy of PLMs on gentle touch sensation (*A*) Schematic of a worm with six touch neurons highlighted in green. The laser paths for imaging (LC 1, green) and severing (LC 2, red) the bottom PLM neuron are shown. (*B*) Confocal images of a PLM neuron labeled with P*mec-7*-GFP (*muls32*) after axotomy or ablation at the L4 stage. The position of the axotomy or ablation is indicated by an orange arrow. White arrows indicate the distal ends disconnected from the cell body. *Insets* show an enlarged view of the synaptic branch, with white arrowheads pointing to the branches (magnification: 2×). In case of ventral branch cutting plus axotomy, the yellow arrowhead points to the absence of the branch. When the PLM was ablated in the L2 stage, the distal axon became degenerated (magenta dotted arrows) at the young-adult stage. (*C*) The bar chart shows the PTRIs and ATRIs measured in worms before and 10 h after axotomy of the PLM at 50 μm from the cell body. Cutting both PLMs has a stronger effect on the PTRI than cutting one PLM, whereas the ATRI remains unaffected. $N = 2$–6 independent replicates. (*D*) PTRI after axotomy on one side at the L4 stage in worms in which the PLM on the other side and the PVM were ablated at the L2 stage. $N = 2$. (*E*) PTRI after axotomy and branch cutting in various combinations. Branch cutting along with axotomy further reduces the PTRI. $N = 2$ or 3. For *C*–*E*, ***$P < 0.0001$; ANOVA with Newman–Keuls multiple comparisons test. The numbers in each bar indicate the number of sides tested. Error bars represent SEM. ns, not significant.

30% of the response (Fig. 1*E*). Then we found that cutting the branch (yellow arrowhead in Fig. 1*B*) along with axotomy reduced the PTRI to 0.21 ± 0.01, which is comparable to the PTRI in animals lacking the mechanosensory channel MEC-4 (Fig. 1*E*). When we ablated PLM cell bodies at the L2 stage, we found that in the young-adult stage the distal axon is completely degenerated (broken purple arrows in Fig. 1*B*), and the PTRI value dropped to 0.18 ± 0.02 (Fig. 1*E*). Hence, these experiments suggested that, after axotomy, the distal axon partly contributes to the residual response. The rest of the response is contributed by the gap junction near the cell body (24). Nevertheless, these results show that the axotomy-induced drop in PTRI is due to the failure in communication mediated by the PLM gap junction and synapse.

Axonal Fusion Between the Proximal and Distal Ends Drives Functional Recovery. The PTRI value following axotomy serves as a baseline to investigate functional recovery over time. We found that the PTRI at 24 h is 0.65 ± 0.01 (mean ± SEM), significantly higher than the PTRI at 10 h postaxotomy (0.52 ± 0.008) (***$P < 0.0001$; Newman–Keuls multiple comparisons test) (Fig. 2*B*). We found that about 42% of the regrowing axons reconnect with their corresponding distal fragments by self-fusion of proximal and distal fragments (Fig. 2 *A*, *b′* and *c′*), as reported previously (9, 14, 15). The rest of the axons regrow toward the distal ends but fail to connect to their respective distal fragments (Fig. 2 *A*, *a′*) (9, 20). We asked whether there would be a difference in PTRI between these two classes, fusion and nonfusion. We separated the fusion class into two subclasses, one that joins end-to-end, called "type 1" (T1), and the other that joins end-to-side, called "type 2" (T2) (Fig. 2 *A*, *b′* and *c′*). The PTRIs measured from the sides showing T1 and T2 fusion were 0.74 ± 0.012 and 0.73 ± 0.016, respectively (Fig. 2*C*). These values were significantly higher (***$P < 0.0001$; Newman–Keuls multiple comparisons test) than the PTRI of 0.54 ± 0.010 found in the nonfusion class (Fig. 2*C*). The average index of the nonfusion class was same as that found at 10 h postaxotomy (Fig. 2*C*). This indicated that the touch response is significantly recovered in animals in which severed axons could fuse to their distal counterparts. A similar observation was made in a different transgenic reporter background, *tbIs222* (P*mec-4*-mCherry) (Fig. S2 *A* and *B*). To check whether the behavioral recovery in the animals in the fusion category is truly due to fusion or to some other compensatory mechanism, we axotomized PLM neurons twice (Fig. 2*D*). The first axotomy was done at the L4 stage, and 24 h later, we picked the worms showing fusion events to perform the second axotomy (Fig. 2*D*). We found that the PTRI at 24 h increased from 0.52 ± 0.008 to 0.76 ± 0.015 in worms showing T2 fusion (Fig. 2*E*). Then, upon the second axotomy, the PTRI dropped significantly, down to 0.45 ± 0.014 (***$P <$ 0.0001; Newman–Keuls multiple comparisons test).

As fusion leads to functional recovery, we expected that the mutants impaired in fusion would display poor recovery. We axotomized the mutants lacking the fusogen molecule EFF-1 (9, 28), the phosphatidyl serine receptor PSR-1 (15), and the ABC transporter CED-7, which is involved in cell engulfment (9, 15).

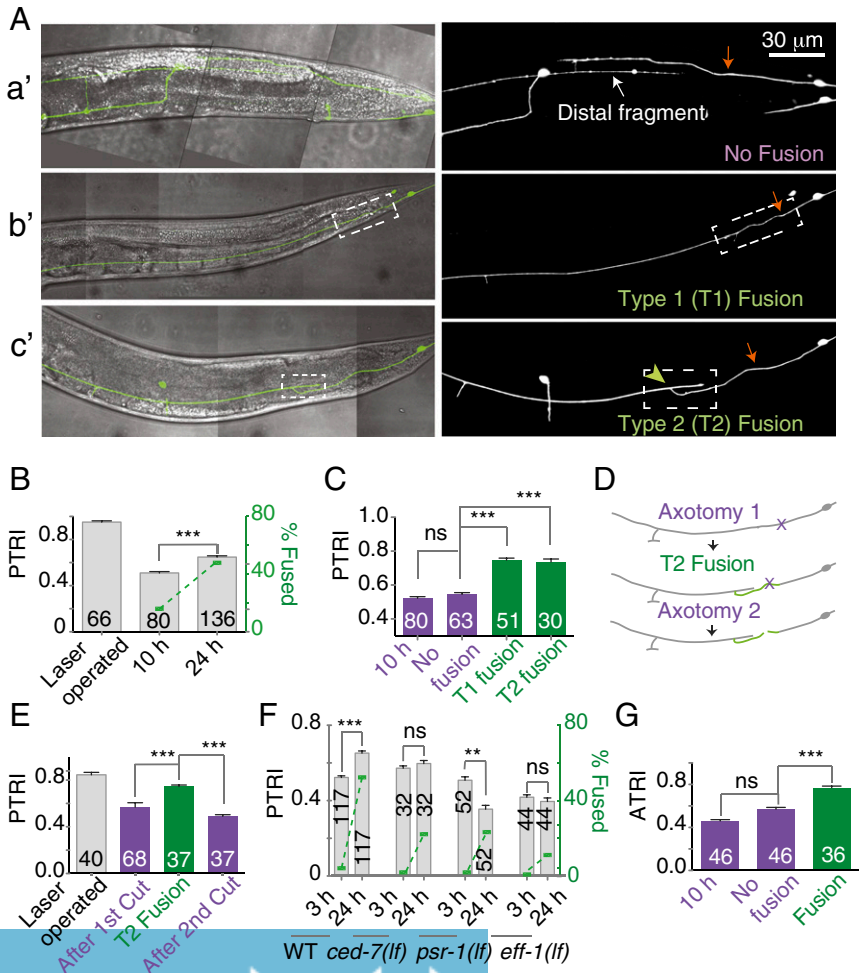

Fig. 2. Fusion between the proximal and distal fragments promotes recovery. (*A*) The confocal images merged with the brightfield differential interference contrast showing three different types of regrowth patterns at 24 h after axotomy: *A*, *a′* shows regrowth without fusion; *A*, *b′* shows T1 fusion; and *A*, *c′* shows T2 fusion. The white dashed box indicates the fused region, and the green arrowhead indicates the point of fusion. (*B*) The double-axis plot represents PTRI on the left *y* axis and the percent fusion on the right *y* axis at 10 and 24 h after axotomy. At 24 h after axotomy, both the percentage of fusion events and PTRI increased. $N = 3$–6 independent replicates. (*C*) PTRI measured in the worms showing nonfusion, T1 fusion, and T2 fusion revealed that the PTRI of fusion events was significantly higher. $N = 6$. (*D*) Schematic representation of the experiment in which axotomy was performed twice on the same PLM. (*E*) Bar graph presenting the PTRI values obtained at different time points in the double-axotomy experiment. $N = 2$. (*F*) The double-axis bar chart presents the PTRI and percent fusion values measured in wild-type, *ced-7 (lf)*, *psr-1(lf)*, and *eff-1(lf)* strains at 3 and 24 h postaxotomy. These mutants show poor functional recovery. $N = 2$–7 independent replicates. (*G*) Fusion events in the ALM lead to recovery of the ATRI. $N = 2$. In *B*–*E* and *G*, ***$P < 0.0001$; ANOVA with Newman–Keuls multiple comparisons test. In *F*, ***$P < 0.0001$, **$P < 0.001$; paired *t* test. The number within each bar indicates the number of sides tested. Error bars represent SEM. ns, not significant.

Each of these genes is important for the axon fusion process (9, 15). We found that these mutants showed a significantly lower percentage of fusion (Fig. 2*F* and Table S1), and their respective PTRIs did not increase significantly at 24 h postaxotomy (paired *t* test) (Fig. 2*F*). In the *psr-1(lf)* strain there was a further drop in PTRI at 24 h postaxotomy (Fig. 2*F*), most likely caused by the enhanced degeneration of the distal ends (white arrows in Fig. S2*F*), which was reported previously (15). The mutants blocked in regeneration, such as *dlk-1*, *pmk-3*, and *ebp-1*, also showed very little rise in their respective PTRIs at 24 h postaxotomy (Fig. S2 *C*–*E*). Similarly, after the axotomy of ALMs, we found that the PTRI value corresponding to the fusion class is significantly higher than the value belonging to the nonfusion class (***$P <$ 0.0001; Newman–Keuls multiple comparisons test) (Fig. 2*G*). These experiments indicated that axonal fusion is the main reason for the improvement in the functional index during the course of regeneration.

Loss of *let-7* Promotes Axonal Fusion and Functional Restoration. Previous studies have identified molecular pathways that inhibit axon regrowth (11, 12, 29). Mutations in these genes accelerate the regrowth process (11, 12, 29). We asked whether any of these mutants would promote functional recovery. To compare recovery across various mutants, we expressed functional recovery as fraction of recovery (FR). FR was obtained by normalizing the gain in PTRI at 24 h due to regeneration over the loss in PTRI after axotomy (*Supporting Information*). The wild-type control showed an FR value of 0.12 ± 0.02 (mean ± SEM). Among the mutants we tested, a significant enhancement in recovery value, 0.28 ± 0.02 (***$P <$ 0.0001; Newman–Keuls multiple comparisons test), is seen in the *let-7(lf)* mutant (Fig. 3*A*). We also tested this in a temperature-sensitive allele, *n2853ts*, of *let-7*. We found that at the restrictive temperature of 20 °C the fusion events increased significantly (Fig. 3*B*), and the FR value increased significantly to 0.40 ± 0.03 from 0.11 ± 0.03, as observed at 15 °C (***$P <$ 0.0001; Newman–Keuls multiple comparisons test) (Fig. 3*C*). The enhanced recovery in the *let-7(lf)* mutant was also reproduced in a different marker background, *tbIs222* (Fig. S3*A*). At every time point we tested, the *let-7(lf)* mutant showed significantly higher PTRI values than the wild-type control (Fig. 3*D*). The percentage of fusion events was also significantly enhanced at similar time points in the *let-7(lf)* mutant (***$P <$ 0.0001; Fisher's exact test). For example, the wild-type strain and the *let-7(lf)* mutant showed 4% vs. 32%, 16% vs. 46%, and 42% vs. 67% fusion at the 3-, 10-, and 24-h time points, respectively (Fig. 3*E*). We further asked whether enhanced fusion events in the *let-7(lf)* mutant are due to the cell-autonomous function of *let-7* miRNA. We expressed the sequence for *let-7* miRNA under the control of either the touch neuron-specific promoter P*mec-4* or the epidermal promoter P*dpy-7* using extrachromosomal arrays. We found that only the transgenic lines *shrEx11* and *shrEx12* that are expressed in touch neurons rescue the enhanced fusion and functional restoration phenotype in *let-7(lf)* (Fig. 3 *E* and *F*). However, epidermal expression of *let-7* rescued neither the axonal fusion phenotype (Fig. 3*E*) nor the FR phenotype (Fig. 3*F*). This suggested that the enhanced fusion and functional recovery seen in the *let-7(lf)* mutant is due to the cell-autonomous effect of *let-7* miRNA. Overexpressing *let-7* in a touch neuron in the wild-type background reduced the fusion events and the FR strongly (Fig. 3 *E* and *F*).

As both axon fusion and regrowth are the outcomes of axotomy, one can argue that the enhanced fusion events in the *let-7(lf)* mutant are the outcome of its increased ability to regrow. To verify this, we tested other mutants that showed enhanced total regrowth in our previous study (11). One such mutant is *efa-6(lf)*, which showed enhanced regrowth due to increased microtubule growth (11, 30). The total regrowth of nonfusion events at 24 h postaxotomy in the *let-7(lf)* mutant is 94.4 ± 5.2 μm (mean ± SEM), which is significantly higher than the 75.2 ± 3.84 μm obtained from the wild-type control (*$P <$ 0.01; Newman–Keuls multiple comparisons test) (Fig. S3 *B* and *C*). Even at 6 h postaxotomy, the elongation in *let-7(lf)* mutants is significantly higher (Fig. S3*C*), and there are more filopodia-like structures at the axon tip (white arrowheads in Fig. S3 *B* and *D*). Nonfused axons in the *efa-6(lf)* mutant showed a total regrowth of 103.0 ± 11.35 μm at 24 h (**$P <$ 0.001; Newman–Keuls multiple comparisons test). However, the fusion frequency in *efa-6(lf)* was 17%, significantly lower than in the control (42%) (***$P <$ 0.0001; Fisher's exact test) (Fig. S3*C*). Other mutants that were reported to show enhanced total regrowth, e.g., *atfs-1(lf)*, *vab-19(lf)*, and *slt-1(lf)*, displayed 12%, 25%, and 46% fusion events, respectively. These rates are either lower than or comparable to the fusion events in the wild-type strain (Table S1). This suggests that fusion and total axon outgrowth are not necessarily linked phenomena.

Our observation that *let-7(lf)* enhances the total regrowth of nonfused PLM axons complements the previous report that *let-7(lf)* promotes the regrowth of the anterior ventral microtubule (AVM) (29). To verify whether AVM neurons also showed fusion-like phenomena, we cut the AVM neuron at 60 μm from the cell body at the L4 stage (orange arrow in Fig. S3*E*) and observed that 45% of the neurons showed fusion (green arrowhead in Fig. S3*F*). This percentage is enhanced to 65% in *let-7(lf)* mutants (*$P <$ 0.01; Fisher's exact test). Therefore, the activity of *let-7* in regulating regeneration responses is similar in PLM and AVM neurons.

***let-7* Regulates Axon Fusion Through *ced-7*.** Previous studies indicated that axon fusion is mediated by the fusogen molecule EFF-1 (9, 15) and is promoted by cell-recognizing mechanisms involving CED-7 and PSR-1 (15). Therefore, we asked whether the enhanced fusion events in the *let-7(lf)* mutant can opt any parallel pathway or rely on the above-mentioned factors. The frequency of fusion events in *ced-7(lf)*; *let-7(lf)* mutants is 22%, similar to the 24% observed in *ced-7(lf)* mutants (Fig. 4*A*). Similarly, the fusion frequency in *eff-1(lf)*; *let-7(lf)* mutants was same as in *eff-1(lf)* mutants (Fig. 4*A*). The enhanced FR in *let-7(lf)* is completely dependent on either *eff-1* or *ced-7* (Fig. 4*B*). This genetic epistasis indicates that *let-7* miRNA, either directly or through its targets, regulates the molecules required for axonal fusion during regeneration.

let-7 miRNA binds and degrades the mRNA of *lin-41* at the L4 stage and helps the developmental transition from larval to adult stage (31, 32). This antagonistic relationship was applied to the regrowth of AVM axons after laser injury (29). FRs in *lin-41(lf)* and *lin-41(lf)*; *let-7(lf)* mutants were not significantly different: −0.029 ± 0.043 (mean ± SEM) and −0.03 ± 0.049, respectively (Fig. 4*B*). FR values in each of these backgrounds are significantly lower than the values in *let-7(lf)* mutants (***$P <$ 0.0001; Newman–Keuls multiple comparisons test). *lin-41* was epistatic to *let-7* for the axonal fusion phenotype as well (Fig. 4*A*).

To test whether *let-7* directly or through the *lin-41* pathway regulates the mRNA level of any of the molecules required for axonal fusion, we used the qRT-PCR approach. We tested the mRNA level of fusogen genes in *let-7(n2853ts)* mutants, which show an elevated level of *lin-41* transcript at the restrictive temperature of 25 °C (33). To determine the fold change in the mRNA level of the genes tested, we normalized the level changes in the wild-type strain as 1 (33, 34) (see *Materials and Methods* for details). We found a 2.23 ± 0.28-fold (mean ± SEM) ($2^{-\Delta\Delta CT}$) increase in *lin-41* level (***$P = 0.0005$; unpaired *t* test with Welch's correction) in the *let-7(n2853ts)* background (Fig. 4*C*) when L1 worms were kept at a nonpermissive temperature (25 °C) for 29 h before RNA preparation. Among the genes tested, we found that the level of *ced-7* mRNA is higher by 1.53 ± 0.11-fold in the *let-7(n2853ts)* strain compared with the wild-type background (***$P = 0.0003$; unpaired *t* test with Welch's correction) (Fig. 4*C* and Table S2). However, we found that the *ced-7* level

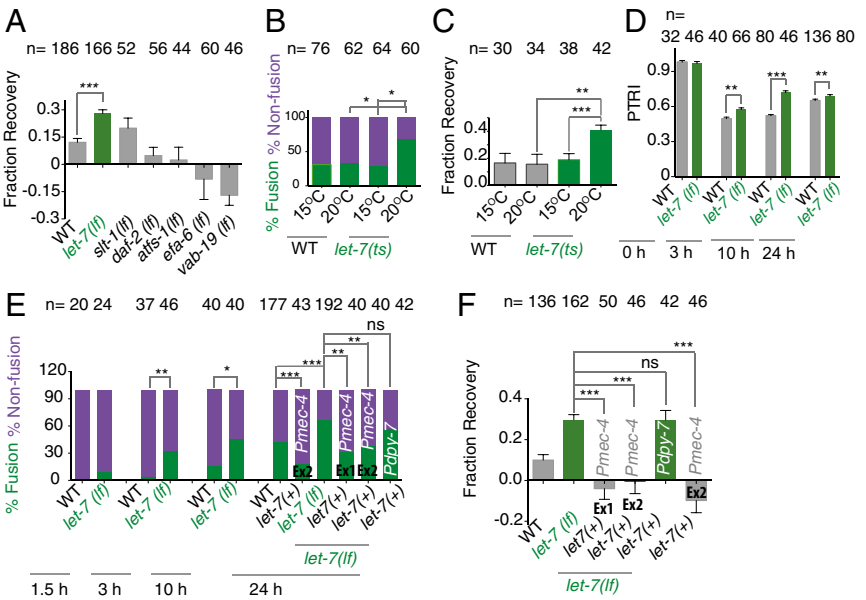

Fig. 3. Loss of *let-7* promotes recovery by increasing the frequency of fusion events. (*A*) The bar chart presents the FR values in mutants lacking different regeneration-inhibiting genes in the *muIs32* (P*mec-7*-GFP) background. *let-7(lf)* shows a significantly high FR. $N = 2–7$ independent replicates. (*B* and *C*) The percent fusion (*B*) and FR values (*C*) in a temperature-sensitive mutant, *let-7(n2853ts)*. *let-7(ts)* worms were grown at 15 °C and were shifted to 20 °C after axotomy. At 20 °C, *let-7*(*n2853ts*) worms show a significantly higher fusion rate and FR. In both *B* and *C*, $N = 2$. (*D*) Comparisons of PTRI in wild-type and *let-7(lf)* worms at different time points after axotomy. $N = 2–5$ independent replicates. (*E*) Fusion percentage in wild-type and *let-7(lf)* worms at different time points after axotomy. Two transgenic lines, *shrEx11* (Ex1) and *shrEx12* (Ex2) expressing *Pmec-4-let-7*, but not *shrEx62* expressing P*dpy-7-let-7*, rescue the increased fusion rate in *let-7(lf)* worms. $N = 2–8$ independent replicates. (*F*) The FR value in *let-7(lf)* is rescued only by touch neuron-specific expression of *let-7*. $N = 2–7$ independent replicates. In *A*, *C*, and *F*, $^{**}P < 0.001$; $^{***}P < 0.0001$; ANOVA with Newman–Keuls multiple comparisons test. In *B* and *E*, $^{*}P < 0.01$; $^{**}P < 0.001$; $^{***}P < 0.0001$; Fisher's exact test. In *D*, $^{*}P < 0.01$; $^{**}P < 0.001$; $^{***}P < 0.0001$; unpaired *t* test with Welch's correction. In *A*, *C*, *D*, and *F*, *n* = the number of sides tested. In *B* and *E*, *n* = the number of axons. Error bars represent SEM. ns, not significant.

remained unaffected in the total loss-of-function mutant *lin-41* (Fig. 4*D*). This indicated that *let-7* regulates the expression of *ced-7* independently of the *lin-41* pathway. While searching for a potential binding site for *let-7* miRNA in genes controlling axon fusion during regeneration, we found that the 3′ UTR of *ced-7* contains a sequence resembling the *let-7* complementary site (LCS) in the 3′ UTR of *lin-41* (Fig. S4*A*) (31, 33, 35). Independently, by in silico prediction using miRNA-mirSVR (www.microrna.org/microrna/home.do) and Target (www.targetscan.org) scans, we found that the UTR of *ced-7* contains a putative LCS, 5′-aacatgcataatacctcg-3′ (Fig. 4*E*). To evaluate the role of *let-7* miRNA in regulating the *ced-7* UTR region, we designed a sensor expressing GFP in touch neurons with the control of the UTR of the *ced-7* gene (Fig. 4*E*). We found that the GFP level in the touch neuron is relatively low (arrow in Fig. 4*F*) in 10 transgenes, each made using a concentration ranging from 1–10 ng/uL. To compare the GFP intensity in the PLM cell body in different strains, we examined the GFP/mCherry ratio expressed in same neuron under the control of the 3′ UTR of *unc-54*. In *let-7(mg279lf)* and *let-7(n2853ts)* mutants, the GFP/mCherry ratios were 0.47 ± 0.04 and 0.64 ± 0.08, respectively. These values are significantly higher than the ratios of 0.28 ± 0.02 and 0.26 ± 0.03 obtained from their respective controls ($^{***}P < 0.0001$; Newman–Keuls multiple comparisons test and $^{**}P = 0.003$; unpaired *t* test with Welch correction, respectively) (Fig. 4 *F* and *G*). Conversely, overexpression of the *let-7* miRNA sequence in

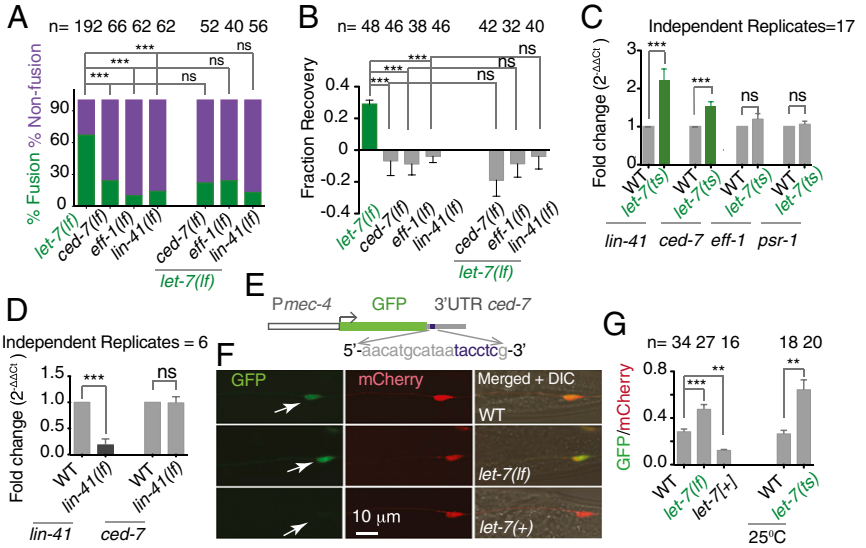

Fig. 4. *let-7* regulates axonal fusion at the L4 stage by downregulating the level of *ced-7* mRNA. (*A* and *B*) Bar charts showing values of percent fusion (*A*) and FR (*B*) in the single mutants *eff-1(lf)*, *ced-7(lf)*, and *lin-41(lf)* and in these mutants individually combined with *let-7(lf)*. In *A*, $N = 3–8$ independent replicates; $^{***}P < 0.0001$; Fisher's exact test; *n* = the number of axons. In *B*, $N = 2$; $^{***}P < 0.0001$; ANOVA with Newman–Keuls multiple comparisons test; *n* = number of sides. (*C*) Bar chart showing the fold change ($2^{-\Delta\Delta Ct}$) in *lin-41*, *ced-7*, *psr-1*, and *eff-1* mRNA levels in *let-7(n2853ts)* mutants at 25 °C. The relative change in mRNA level was normalized to *tba-1* (*Materials and Methods*). Three technical replicates were run for each gene tested in each of the biological replicates mentioned. $^{***}P = 0.0008$; unpaired *t* test with Welch's correction. (*D*) Fold change ($2^{-\Delta\Delta Ct}$) in *lin-41* and *ced-7* mRNA levels in *lin-41 (ma104)* mutants using the method described above. Three technical replicates were run for each gene tested in each of the biological replicates mentioned. $^{***}P \leq 0.0005$; unpaired *t* test with Welch's correction. (*E*) The design of the GFP reporter with the 3′ UTR of *ced-7*. The expanded sequence represents the putative LCS in the 3′ UTR of *ced-7*. (*F*) Confocal images of the PLM cell body showing the expression of *shrEx72* (P*mec-4*-GFP-3′ UTR *ced-7*) (white arrows) and *tbIs222* (P*mec-4*-mCherry-3′ UTR *unc-54*) as an internal control. Upon *let-7* overexpression, the GFP intensity goes down. (*G*, *Left*) The bar chart compares the relative GFP/mCherry intensity in the *let-7(lf)*, *shrEx12* [P*mec-4-let-7*(+)], and wild-type strains. $N = 1–4$ independent replicates. $^{***}P < 0.0001$, $^{**}P < 0$; ANOVA with Newman–Keuls multiple comparisons test. (*Right*) the GFP/mCherry values in the *let-7(n2853ts)* strain at 25 °C. $^{**}P = 0.0021$; unpaired *t* test with Welch's correction. *n* = the number of PLM cell bodies. Error bars represent SEM. ns, not significant.

touch neurons reduces the GFP/mCherry ratio from 0.28 ± 0.023 to 0.12 ± 0.007 (**$P < 0.001$; Newman–Keuls multiple comparisons test) (Fig. 4 *F* and *G*). The mCherry intensity in the cell body mostly remained constant in these backgrounds having different doses of *let-7* (Fig. S4*C*). These results suggest that the loss of *let-7* promotes axonal fusion by increasing the *ced-7* level, most likely independently of the *lin-41* pathway, and that the *ced-7* mRNA level could be regulated by *let-7* through its UTR sequence. However, they counter the evidence that *lin-41(lf)* reduces axonal fusion. Loss of *lin-41* reduced the initiation of axon regrowth in AVM neurons (29). We also found that in the *lin-41(lf)* strain the regrowth of the PLM is strongly reduced ($P < 0.0001$, Newman–Keuls multiple comparisons test) (Fig. S4 *D* and *E*). Frequently, axons fail to initiate regrowth even at 24 h after axotomy (Fig. S4*D*). If regrowth is strongly perturbed, axon fusion will also be perturbed, as seen in the *ebp-1(lf)* and *dlk-1(lf)* mutants.

Loss of *let-7* Helps Overcome the Aging-Related Decline in Regeneration by Promoting Effective Fusion Events. It is known that the axon regeneration potential declines with age in worms (13, 20, 36, 37) and other organisms (38, 39). We tested how functional restoration would be affected by aging and whether *let-7* miRNA would influence any of the parameters of axon fusion in an age-dependent manner. We measured the PTRI at different ages: L4 (late larva), A2–A5 (days 2–5), A7 (day 7), A8 (day 8), A11 (day 11), and A16 (day 16), and found a significant reduction in PTRI from A5 onwards (Fig. S5). We chose worms at the A3 and A4 stages for our experiment, as the basal PTRIs at these stages were not altered (Fig. S5). We found that the FR in animals operated at the A3 and A4 stages are −0.02 ± 0.02 and −0.04 ± 0.023 (mean ± SEM), respectively, which are significantly lower (***$P < 0.0001$; Newman–Keuls multiple comparisons test) than the FRs of 0.14 ± 0.031 found in animals operated at the L4 stage (Fig. 5*A*). However, the fusion events were not reduced at A3 or A4 (Fig. 5*B*). This raised a question whether the fusion events in the old animal are functional or not. To answer this, we compared the FR values between fusion and nonfusion groups (Fig. 5*C*). As noticed earlier, in the L4 stage the FR in the fusion events is 0.42 ± 0.029, significantly higher (***$P < 0.0001$; Newman–Keuls multiple comparisons test) than the value of −0.013 ± 0.03 in the nonfusion events (Fig. 5*C*). However, at the A3 and A4 stages the FR values in the fusion category were not significantly higher than those in the nonfusion class (Fig. 5*C*). This indicated that for some reason the fusion events in old animals are not effective in repairing the lost function. Similar experiments in *let-7(lf)* mutants revealed that there is no drop in recovery values in the A3 and A4 stages (Fig. 5*A*). The FRs at the L4, A3, and A4 stages were 0.25 ± 0.042, 0.26 ± 0.045, and 0.23 ± 0.036, respectively. These values were significantly higher than the values in the wild-type strain (***$P < 0.0001$; Newman–Keuls multiple comparisons test) (Fig. 5*A*). Also, in the *let-7(lf)* mutant, the FR values for fusion class at the A3 and A4 stages remained significantly than those of nonfusion class (Fig. 5*C*). This indicated that the loss of *let-7* overcomes the age-related decline in functional restoration through effective axon fusion. Conversely, when we overexpressed *let-7* in touch neurons, the FR at L4 becomes −0.098 ± 0.059, significantly lower (***$P < 0.0001$; Newman–Keuls multiple comparisons test) than the value in the wild-type strain at same stage and comparable to the FR value in the worms axotomized at the A3 stage. Therefore, *let-7* is sufficient to induce aging-like symptoms, such as the lack of functional restoration, in the late larval stage. On the other hand, the *daf-2(lf)* mutant, which has increased life span due to the down-regulation of insulin signaling, showed no enhancement in fusion events or in functional recovery (Fig. 5 *A* and *B*).

Loss of *let-7* Restores Age-Dependent Vesicular Transport and Helps Enrichment of EFF-1 in the Growing Tip. We speculated that in aged worms, although injured axons showed fusion-like phenomena at the anatomical level, the cytoplasmic continuity is not established. To test this, we used in vivo imaging of Rab-3 protein tagged with GFP (GFP::RAB-3) to study axonal transport (40, 41). We imaged bidirectional movement of RAB-3 particles (Fig. 6 *A*, *a′* and *b′* and Movie S4*A*) in the proximal and distal ends in fused axons (Movie S4*A*). We present the GFP::RAB-3 dynamics in given regions of interest (ROIs) (Fig. 6 *A*, *a′* and *b′*) as a kymograph (Fig. 6 *C* and *D*). In a kymograph (Fig. 6*C*), diagonal tracks represent events of anterograde or retrograde movement. We present the movement as particle flux, i.e.,the number of moving particles per unit length of axon per unit of time, as described before (41). We reasoned that a successful fusion event would lead to cytoplasmic continuity between the proximal and distal ends, and therefore, the particle flux in the distal and proximal ends will be similar. The values of anterograde and retrograde particle flux in the proximal fragment were 0.016 ± 0.0015 particles·μm^{-1}·s^{-1} and 0.0078 ± 0.0013 particles·μm^{-1}·s^{-1} (mean ± SEM), respectively, in T2 fusion events (Fig. 6 *A*, *a′*). In the distal pare, these values were 0.013 ± 0.001 particles·μm^{-1}·s^{-1} and 0.007 ± 0.0009 particles·μm^{-1}·s^{-1}, respectively, (Fig. 6*E*), similar in range to those in the proximal part. After the region of fusion was photobleached, the movement of particles through the point of fusion became much clearer (Movie S4*B*). In nonfusion events (Fig. 6 *A*, *b′*), the values of anterograde and retrograde flux in distal end axons were 0.0012 ± 0.0002 particles·μm^{-1}·s^{-1} and 0.0011 ± 0.0004 particles·μm^{-1}·s^{-1}, respectively, indicating that the Rab-3 particles are relatively static in the distal end (Fig. 6 *D* and *E* and Movie S6). Flux was significantly higher in the proximal part (***$P < 0.0001$; Newman–Keuls multiple comparisons test) (Fig. 6 *D* and *E* and Movie S5). The PTRI values corresponding to the fused and nonfused events in this experiment were 0.75 ± 0.01 and 0.48 ± 0.04, respectively, and they differed significantly (***$P < 0.0001$; Newman–Keuls multiple comparisons test). Therefore we found a correlation among fusion events, restoration of particle flux in the distal end, and functional recovery. We noticed that in A3 worms the steady-state value of anterograde flux is significantly reduced (**$P < 0.001$; Newman–Keuls multiple comparisons test) (Fig. S6*B*), and this value is significantly higher in *let-7(lf)* mutants (***$P < 0.0001$; Newman–Keuls multiple comparisons test) (Fig. S6 *A* and *B* and Table S3). This indicated that there is improved axonal transport in *let-7(lf)* mutants, most likely due to delayed neuronal aging.

In T2 fusion events at the A3 stage, we found that there is very little movement of RAB-3 particles in a given distal end (Fig. 6*F* and Fig. S6*C* and Movie S7). For example, anterograde particle flux in the distal end was 0.0023 ± 0.0004 particles·μm^{-1}·s^{-1}, as opposed to 0.007 ± 0.0008 particles·μm^{-1}·s^{-1} in the proximal end (***$P < 0.0001$; Newman–Keuls multiple comparisons test) (Fig. 6*F*). This indicated that transport is not restored in the distal end due to insufficient cytoplasmic continuity between the proximal and distal ends. However, the RAB-3 particles in the distal end of fused axons at the A3 stage in the *let-7(lf)* mutant (Fig. S6*C*) showed significant bidirectional movement (Fig. 6*F* and Movie S9). For example, the anterograde flux values in the proximal and distal ends were 0.0154 ± 0.0015 particles·μm^{-1}·s^{-1} and 0.014 ± 0.0013 particles·μm^{-1}·s^{-1}, respectively.

In older worms, incomplete cytoplasmic continuity might have occurred due to the lack of EFF-1 during the axon fusion process. To test this hypothesis, we developed an EFF-1::mCherry reporter (Fig. 6*G*). This construct is functional, as the axonal fusion in *eff-1(lf)* worms carrying the transgene became 73%, compared with the 10% fusion observed in *eff-1(lf)* worms without transgene (***$P = 0.0001$; Fisher's exact test). We found that at 6 h postaxotomy, the EFF-1::mCherry signal is upregulated near the growing end of axons (dashed box, R-I in Fig. 6*G*). Imaging the region near the growth cone reveal that EFF-1 is present throughout the growth cone but is also enriched at the tip of the filopodia-like protrusions (arrows in Fig. S7*A*). The GFP::RAB-3 puncta are also enriched at the growth cone

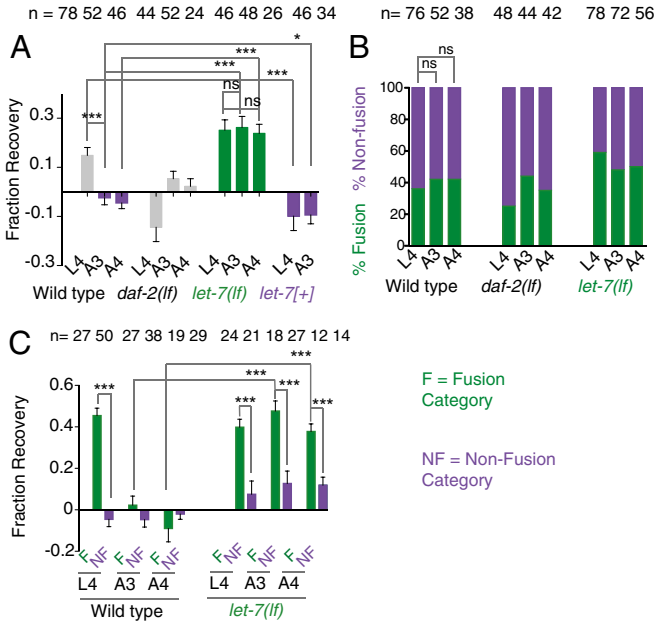

Fig. 5. Loss of *let-7* overcomes the age-related decline in functional recovery. (*A*) FR values at 24 h postaxotomy at the L4, A3, and A4 stages. *let-7(lf)* shows significantly high recovery in all stages. *let-7* overexpression using *shrEx12* [P*mec-4-let-7(+)*] reduces the FR independently of age. $N = 2$ or 3 independent replicates. (*B*) The bar plot represents fusion percentages at 24 h in control, *daf-2(lf)*, and *let-7(lf)* strains after axotomy at different stages. $N = 2$–4 independent replicates. (*C*) FR values corresponding to the fusion (F) and nonfusion (NF) classes were compared after axotomy at different ages. In control worms, the fusion class shows a significantly higher FR only at the L4 stage. In *let-7(lf)* worms the fusion class shows significantly higher FR values than the nonfusion class at all stages. $N = 2$ or 3. In *A* and *C*, $^{*}P < 0.01$; $^{***}P < 0.0001$; ANOVA with Newman–Keuls multiple comparisons test. For each bar, n = the number of sides tested. In *B*, ns, not significant; Fisher's exact test. n = the number of axons. Error bars represent SEM.

(arrows in Fig. S7*A*). To quantify this phenomenon, we measured the intensity of EFF-1::mCherry in two 10-μm ROIs, one, R-I, near the growing tip (Fig. 6*G*) and the other, R-II, placed 10 μm away (Fig. 6*G*). The average intensities of EFF-1::mCherry in R-I and R-II at 30 min after axotomy were 69.28 ± 21.11 (mean ± SEM) and 61.58 ± 13.37, respectively. After 6 h these values rose to 165.2 ± 21.14 and 104.1 ± 12.82 (Fig. 6*H*) in R-I and R-II, respectively ($^{*}P < 0.01$, $^{**}P < 0.001$; Newman–Keuls multiple comparisons test). The signaling intensity was significantly higher in R-I than in R-II ($^{***}P < 0.0001$; Newman–Keuls multiple comparisons test) (Fig. 6*H*), indicating an EFF-1::mCherry gradient with the highest concentration at the growth cone, which is in agreement with previous observation (15). The intensity of GFP measured as an internal control in the above-mentioned ROIs never increased after axotomy (Fig. S7*B*). Similar experiments in A3 worms revealed that the intensity of EFF-1::mCherry in R-I at 6 h postaxotomy is significantly lower than the value obtained at the L4 stage ($^{*}P < 0.01$, $^{**}P < 0.001$; Newman–Keuls multiple comparisons test). The value in R-I is not significantly higher than that in R-II (Fig. 6*H*), indicating that the enrichment of EFF-1::mCherry at the growth cone is diminished in the A3 stage. We found that the loss of *let-7* increased the intensity of EFF-1::mCherry in R-I (arrowhead, Fig. 6 *G* and *H* and Fig. S7*D*). The average intensity in R-I, 151.1 ± 31.76, was significantly higher than that in R-II, 85.52 ± 22 ($^{**}P < 0.001$; Newman–Keuls multiple comparisons test). We concluded that the loss of *let-7* improves the enrichment of EFF-1 at the growing tip, possibly due to the enhanced axonal transport seen in this background.

If EFF-1 is limiting at the growing tip of axons for functional repair, increasing the level of EFF-1 might be sufficient to obtain functional fusion events in aged worms. We performed axotomy on aged worms expressing a functional EFF-1::mCherry transgene (*shrEx59*) and found that at A3 and A4 the FR index of fusion events in these worms (0.35 ± 0.043 and 0.24 ± 0.035 respectively) is higher than the respective indices in wild-type worms (0.02 ± 0.05 and −0.029 ± 0.02, respectively) (Fig. 6*I*). Also the FR values corresponding to the fusion category in the A3 and A4 stages remained significantly higher ($^{*}P < 0.01$, $^{***}P < 0.0001$; Newman–Keuls multiple comparisons test) than the values of nonfusion classes in the *eff-1*(+) background (Fig. 6*I*). This evidence suggested that the EFF-1 concentration is limiting for the functional restoration in old worms. The loss of *let-7* overcomes this barrier by enhancing the axonal transport and enriching EFF-1 protein in the growing tip of the axon.

Discussion

C. elegans mechanosensory neurons have long been used to understand the molecular pathways controlling their regrowth ability. In this study, we directly address the functional consequences of the regeneration patterns. Our data reveal that the axon fusion is the major phenomenon that drives functional regeneration in touch neurons.

Use of Multiple Femtosecond Lasers in Neurosurgery. Our analysis with this multilaser system reveals that cutting both sides has a severe effect on gentle touch sensation as opposed to cutting one side. This further opens up the possibility of functional analysis of the touch circuit. The functional connectivity of the other neurons, such as PVD, AWC, and ASER, that are located bilaterally in *C. elegans* (23) can be dissected out using this multilaser two-photon system.

We found that, after axotomy, the intact distal end has the ability to give some response. This is consistent with the previous report that severing the axon or ablating the cell body alone in a microfluidic device has less effect on gentle touch sensation (27). However, the effect is more significant after the removal of the synaptic branch (27). After axotomy, one would imagine that the contribution of the gap junction present near the PLM cell body would be absent. Therefore, gap junction-mediated communication to the PVC, through which the reversal response is generated, would be abolished. The synaptic branch in the distal end makes a synapse to the AVA interneuron (42). It is predicated that AVA might communicate with PVC (24, 43). The synaptic branch within the intact distal end might communicate with the PVC through the AVA. Thus, a worm can respond to a posterior touch without a contribution from the gap junction after axotomy.

Axonal Fusion in Functional Recovery. For functional recovery to occur after neuronal injury, the regenerating axon must establish connectivity with its original target, either by the formation of a chemical synapse to its postsynaptic neuron or by reconnecting with its own distal fragments. In many systems, such as earthworm, *Aplysia*, *C. elegans*, crustaceans, and crayfish, the second phenomenon, known as "fusion" occurs (4–6, 9). In *C. elegans*, fusion during regenerative growth is dependent on the cell-recognition molecules CED-7, the phosphatidylserine receptor PSR-1, and the fusogen molecule EFF-1 (9, 15). In this study, we have correlated the anatomical regrowth patterns with the behavioral recovery in the same animal using microscopy and behavioral tests. We have shown that an efficient fusion restores the axonal transport in the distal end. Therefore, we have provided evidence for cytoplasmic continuity in the case of axon fusion. This undoubtedly proves that fusion could help recover function significantly and provides promising evidence that harnessing the fusion pathways after neuronal injury could be beneficial. Fusion might also protect long axonal tracts from degeneration after small breakages caused by

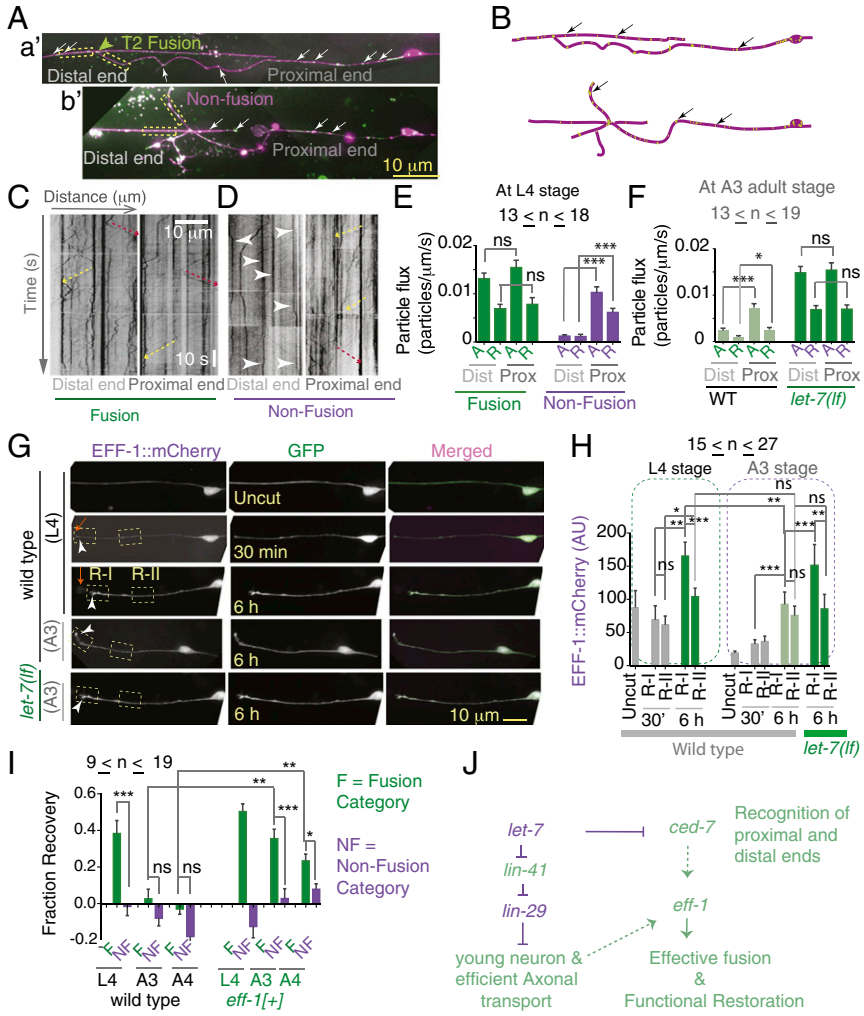

Fig. 6. Loss of *let-7* improves axonal transport during axonal fusion. (*A*, *a*′ and *b*′) Still images from time-lapse movies of the PLM with *tbIs222* (P*mec-4*-mCherry) and *jsIs821* (P*mec-7*-GFP::RAB-3) using spinning-disk confocal at 24 h postaxotomy. mCherry is shown in magenta, and GFP::RAB-3 is shown in green. White arrows indicate GFP::RAB-3 particles in the axon. (*A*, *a*′) T2 fusion. (*A*, *b*′) Nonfusion. (*B*) Schematic representation of images shown in *A*. (*C*) Kymographs from the movies of 180-s duration were generated from the 30-μm ROIs (yellow dotted box in *A*, *a*′) placed on the distal and proximal ends of fused neuron. Diagonal tracks represent events of anterograde (dashed yellow arrow) or retrograde (dashed red arrow) movements. (*D*) A kymograph from the distal and proximal ends of a nonfused axon as shown in *A*, *b*′. The perpendicular tracks (arrowheads) represent static particles. (*E*) The bar chart represents particle flux in the proximal and distal ends measured in fusion and nonfusion events. A, anterograde events; R, retrograde events. Particle flux = number of particles or tracks per micrometer per second. $N = 5$–8 independent replicates. (*F*) The bar chart shows flux values in the proximal and distal ends in A3 worms measured in T2 fusion events. $N = 4$–7 independent replicates. (*G*) Spinning-disk confocal images of worms coexpressing *muIs32* (P*mec-7*-GFP) and *shrEx59* (P*mec-4*-EFF-1::mCherry) before and after axotomy. Orange arrows indicate the site of axotomy. Two ROIs are shown: R-I at the cut tip and R-II placed 10 μm away from ROI-I to quantify the average intensity of EFF-1::mCherry. EFF-1 intensity is increased at R-I at 6 h after axotomy. This enrichment is reduced at the A3 stage. (*H*) The average intensity of EFF-1::mCherry in two ROIs obtained 30 min before and 6 h after axotomy is plotted for L4- and A3-stage experiments. $N = 2$–4 independent replicates. (*I*) In the *eff-1(+)* strain *shrEx59* (P*mec-4*-EFF-1::mCherry), FR values in the fusion category are increased significantly compared with the values in wild-type strain at the A3 and A4 stages. $N = 2$. In *E*, *F*, *H*, and *I*, $*P < 0.01$; $**P < 0.001$; $***P < 0.0001$; ANOVA with Newman–Keuls multiple comparisons test. Error bars represent SEM. (*J*) The working model depicting how the *let-7* miRNA pathway negatively regulates effective axon fusion in L4 and aged worms. ns, not significant.

physical stress. Therefore, this self-repair process might maintain the functional integrity of the nervous system throughout the life span of an organism.

Loss of *let-7* miRNA Promotes Functional Restoration in Adult Animals. Manipulation of intracellular pathways has some promise in giving rise to improved axon regeneration. For example, activation of cAMP messenger signaling, inhibition of the PTEN subunit of the mTOR pathway, and stabilization of the microtubule cytoskeleton have individually helped overcome regeneration blocks in the neurons after spinal cord injury (44–46). By screening mutants of axon regrowth-related genes for functional recovery, we found that *let-7* miRNA negatively regulates functional restoration. Our data indicated that the enhanced functional recovery seen in *let-7* mutants is dependent on the fusogen molecule EFF-1 (28) and on cell-recognition molecules such as PSR-1 and CED-7. *let-7* miRNA inhibits the heterochronic gene *lin-41* and in turn releases the inhibition of the transcription factor LIN-29 to help the developmental transition from L4 to the adult stages (32, 47). Normally *let-7* expression becomes prominent in the late L4 stage, and its level remains high in adult stages. We found that in *let-7(lf)* mutants the mRNA level of *ced-7* is up-regulated in the L4 stage, and the frequency of axon fusion is increased. We further found that the 3′ UTR of *ced-7* has a putative *let-7* miRNA-binding site and that this UTR is sensitive to the dose of *let-7*. This indicated

that *let-7* might target *ced-7* directly by binding to its UTR. Overall, our data suggest that *let-7* negatively regulates the axon fusion process by reducing the mRNA level of *ced-7*.

One intriguing finding is that the correlation between fusion-like phenomena and functional recovery is lost in old worms. Previous work suggested that EFF-1 is enriched near the contact point between the proximal and distal ends during the fusion process (15). We showed that EFF-1 fusogen is limiting at the growing tip of axon in the older worms and is sufficient to establish functional fusion events. We found that axonal transport is affected in older worms, and the enrichment of EFF-1 is also perturbed. So EFF-1 could be transported to the axon tip following neuronal injury.

We propose that *let-7* regulates axon fusion in two ways (Fig. 6*J*). Loss of *let-7* increases the probability of contact between the proximal and distal ends by increasing the level of *ced-7* mRNA. However, *ced-7* is not sufficient to establish cytoplasmic continuity in older animals. In older animals, *let-7(lf)* maintains the healthy bidirectional axonal transport by delaying neuronal aging, and therefore EFF-1 is not limiting at the axon tip. Similarly, the fusogen molecule AFF-1 is limiting in older animals for proper branching of the PVD dendrite during regeneration (48).

Materials and Methods

***C. elegans* Strains.** *C. elegans* strains were grown on nematode growth medium (NGM) agar plates at 20 °C using standard methods (49). For growing the temperature-sensitive mutant *let-7(n2853ts)*, we used a 15 °C incubator as a permissive condition and 20 °C as a nonpermissive condition (31). All the loss-of-function alleles except *let-7(n2853ts)* are denoted as "*lf*". For example, the *dlk-1* mutant is presented as *dlk-1(lf)*. All the strains used for this study are identified in *Supporting Information*.

Femtosecond Lasers, Axotomy, and Imaging. Most of the axotomy experiments other than the experiments involving age-related changes in functional recovery were done at the L4 stage. During axotomy and imaging, the worms were immobilized by using 10 mM levamisole hydrochloride (Sigma L0380000) anesthesia in a 5% agarose pad or with a suspension of 0.1-μm-diameter polystyrene beads (00876-15; Polysciences) in a 12.5% agarose pad in M9 (medium 9) (26). Axotomy and two-photon imaging were performed simultaneously using Bruker Corporation's ULTIMA setup (Fig. S1*A*). The setup is equipped with two tunable (wavelength range: 690–1,040 nm), automated dispersion-compensated femtosecond laser systems from Spectra Physics (Mai Tai with DeepSee). A pair of Conoptics pockel cells was used to control the average laser output with superior (approximately microsecond) temporal resolution. The imaging was performed by a 6-mm scanning galvanometer system; a 3-mm system was used for the axotomy (Fig. S1*A*). A 60× water-immersion objective (NA = 1.1, Olympus) was used for simultaneous imaging and axotomy experiments. GFP was imaged using a 920-nm laser, and a 720-nm laser [pulse width ∼ 80 fs, irradiation pulse width: 20 ms, lateral point spread function (PSF) ∼400 nm, and *z* axis PSF ∼1.5 μm] was used for all axotomy unless otherwise mentioned.

Gentle Touch Assay. For every experiment described in this report, the gentle touch assay was performed on both sides of the worm. Before or at any time point after axotomy, the worms were placed in individual plates. A worm generally lies on one of its sides. The side facing upward was assayed first, and whether it was the right or the left side was noted. In this assay, the worms were subjected to anterior and posterior touch alternatively, 10 times each, with the help of an eyelash tip (50). We denoted response as 1 and no response as 0. To assay the other side, the worms were flipped with the help of the eyelash and were kept undisturbed for 20 min; then the same assay was performed. We calculated the ATRI and PTRI for each side as a ratio of the total number of responses to the total number of touches given (10 touches) (51, 52). For example, we determined both the PTRI and ATRI after cutting PLM cells (Fig. 1*C*). This showed that cutting PLMs reduced only the PTRI, leaving the ATRI unaffected (Fig. 1*C*). For rest of the experiments, which were done on the PLM, only the PTRI was presented. The experimenter was unaware of the genetic background of the worm strains and laser treatment conditions. The method for correlating axonal fusion events with functional recovery is described in more detail in *Supporting Information*.

Molecular Biology and Transgenes. For touch neuron-specific expression of *let-7*, a gateway (Invitrogen) entry clone *let-7* [pCR8:*let-7* (pNBRGWY21)] was constructed by PCR and recombined with pCZGY533 (P*mec-4* destination vector) and pNBRGWY44 (P*pdy-7* destination vector) to generate P*mec-4-let-7* (pNBRGWY16) and P*dpy-7-let-7* (pNBRGWY36), respectively. The primers used for generation of pCR8:*let-7* were 5′-CTACACTGTGGATCCGGTG-3′ and 3′-GCTTCGAAGAGTTCTGTCTC-5′. To make P*mec-4*-EFF-1::mCherry and P*mec-4*-EFF-1::GFP, an entry clone pNBRGWY39 (PCR8:*eff-1*-cDNA) was constructed by PCR using primers 5′-GCCCTTCATGGAACCGCCG-3′ and 5′-GATGTACTGGCTACTGCTATAG-3′. Then the pCR8 plasmid was recombined with pCZGY859 (P*mec-4*-Gateway-mCherry) and pCZGY858 (P*mec-4*-Gateway-GFP) to generate P*mec-4*-EFF-1::mCherry (pNBRGWY41) and P*mec-4*-EFF-1::GFP (pNBRGWY40), respectively. To generate P*mec-4*-GFP-3′ UTR *ced-7*, first the boundary of the UTR was found from the annotated gene sequence of *ced-7* in the Caenorhabditis Genetics Center (CGC) database (https://cbs.umn.edu/cgc/home). Then the UTR was amplified with the forward primer (*ced-7* 3′UTR F) 5′-CGGGATATCCCGTTGCCGGTCTCGACG-3′ and the reverse primer (*ced-7* 3′ UTR R) 5′-CGGACTAGTCCGGCGATCCCAGACAGTGCATTTC-3′ and was cloned into a pCR8 vector to obtain pNBRGWY37 (pCR8: 3′ UTR *ced-7*). Then the pCR8 clone was recombined with pCZGWY1867 (P*mec-4*-GFP-Gateway destination vector) to generate pNBRGWY38 (P*mec-4*-GFP -3′ UTR *ced-7*).

RNA Extraction and qRT-PCR. Standard RT-PCR analyses were performed following previous methods (53). We used RNA samples from L4-staged N2, *let-7(n2853ts)* and *lin-41(ma104)* worms. To prepare RNA samples from *let-7 (n2853ts)* strain, ∼50–80 gravid adult worms grown at 15 °C were allowed to lay eggs for 3–4 h in a 60-mm NGM plate at 15 °C. After hatching, one batch of worms at the L1 stage was transferred and kept at 25 °C for 29 h as described previously (54), and the other batch was kept at 15 °C. *lin-41(ma104)* worms and respective wild-type controls were grown at 20 °C. Then the L4 worms were collected and washed three times in M9 buffer, pelleted down, frozen, and stored at −80 °C. RNA was extracted from the thawed worms using the Qiagen RNeasy Mini Kit (no. 74104; Qiagen). The extracted RNA was then treated with DNase I to remove genomic DNA contamination using Ambion's DNA-free kit (AM1906). cDNA was prepared from ∼2 μg RNA using SuperScript III Reverse Transcriptase (no. 18080093; Thermo Fisher Scientific). Twenty-five nanograms of RNA were used for qRT-PCR in 20 μL of Power SYBR Green PCR Master Mix (no. 3367659; Applied Biosystems Life Technologies). The reactions were performed for 40 cycles. Relative positions of the primers are indicated in Fig. S4*A*, and their sequences are given in *Supporting Information*. Some of the primers were designed for priming at the intron and exon boundary to avoid amplification from contaminated genomic DNA (Fig. S4*A*). The rest were designed so that the genomic DNA contamination would result in a PCR product larger than the reverse transcribed product. However, no contaminating bands were observed in 3% agarose gel, when PCR reactions were run (Fig. S4*B*). The relative mRNA amounts of target genes in the *let-7(n2853ts)* and wild-type strains were calculated using the ΔΔCt method and were normalized to *tba-1* control for endogenous mRNAs (33). The value for wild type was set to one for calculations of fold modulation (33, 34).

Time-Lapse Imaging of GFP::RAB3 and EFF-1::mCherry. The worms were immobilized using 10 mM levamisole hydrochloride on 5% agarose pads. GFP::RAB-3 and mCherry were imaged from worms coexpressing *jsIs821* (P*mec-7*-GFP::RAB-3) (40) and *tbIs222* (P*mec-4*-mCherry). For live imaging of GFP::RAB-3 fluorescence, we collected 535 frames at the rate of three frames/s using the 100× lens of a NA-1.46, Yokogawa CSU-XA1 spinning-disk confocal head and a HAMAMATSU SZK, Japan EMCCD camera (512 × 512) controlled by Velocity software in a spinning-disk system (Perkin-Elmer Ultraview) assembled in an Olympus IX83 microscope.

EFF-1::mCherry and internal control GFP were imaged from the worms coexpressing *shrEx59* (P*mec-4*-EFF-1- mCherry) and *muIs32* (P*mec-7*-GFP). We imaged worms at the L4 and A3 stages, before and after axotomy. EFF-1::mCherry and GFP were imaged using 20% laser power of 561-nm and 488-nm lasers, respectively. We used exposure times of 350 ms and 50 ms for EFF-1::mCherry and GFP, respectively. Imaging was done using a CSU-XA1 scan-head and a Photometric Evolve EMCCD camera (512 × 512) controlled by Zen Blue software in a Zeiss Axio Observer.Z1 microscope. Details of the quantitative measurements of GFP::Rab-3 movement and the intensity of EFF-1::mCherry are provided in *Supporting Information*.

Point-Scanning Confocal Imaging. For quantitative imaging of P*mec-4*-GFP- 3′ UTR *ced-7* (sensor) lines, the worms coexpressing P*mec-4*-GFP- 3′ UTR *ced-7* (sensor) and P*mec-4*-mCherry-3′ UTR *unc-54* (*tbIs222*) were imaged with 60.5% of 488-nm and 43.6% of 543-nm lasers, respectively, under a 100× oil

objective (NA 1.3). Scanning was done with a Zeiss LSM 510 Meta confocal. Two or three z-sections were collected with a scanning speed of 6 and 2× averaging, with detector gain values of 668 and 708 for the 488-nm and 543-nm lasers, respectively. Images were collected below the saturation limit. The average GFP and mCherry intensities were measured in a ROI drawn on the PLM cell body.

EFF-1::GFP: P*mec-4*::EFF-1::GFP was imaged using 68% of a 488-nm laser.

Statistics. Statistical analyses were performed using GraphPad Prism software. For two-way comparisons, an unpaired *t* test with Welch's correction was used. A paired *t* test was performed when comparing the PTRI values obtained at 3 h and 24 h postaxotomy from the same worm. Fisher's exact test was used for proportions. Three or more samples were compared with ANOVA (nonparametric) with a Newman–Keuls multiple comparisons test. In all the bar graphs, we denote "*n*" as the number of samples and "*N*" as the number of independent replicates. The error bars represent the SEM.

ACKNOWLEDGMENTS. We thank National Bio Resource Project, Japan and CGC (supported by the NIH National Center for Research Resources) for strains; Apeksha Supekar for help with the aging experiments; Sourav Banerjee and the members of his laboratory for help with qRT-PCR experiments; and members of the A.G.-R. and S.P.K. laboratories and Bela Desai for discussion and suggestions. A.G.-R. is an Intermediate Fellow of the Wellcome Trust–Department of Biotechnology (DBT) India Alliance. S.D. received technical support from Bruker's Middleton, WI facility. This work is supported by the National Brain Research Center Core Fund of the Department of Biotechnology and Wellcome Trust-DBT India Alliance (Grant IA/I/13/1/500874 to A.G.-R.). Spinning-disk confocal microscopy was supported by DAE-PRISM Grant 12-R&D-IMS-5.02-0202 (to S.P.K.) and a Howard Hughes Medical Institute International Early Career Scientist Award (to S.P.K.).

1. Chew DJ, Fawcett JW, Andrews MR (2012) The challenges of long-distance axon regeneration in the injured CNS. *Prog Brain Res* 201:253–294.
2. Liu K, Tedeschi A, Park KK, He Z (2011) Neuronal intrinsic mechanisms of axon regeneration. *Annu Rev Neurosci* 34:131–152.
3. Luo L, O'Leary DD (2005) Axon retraction and degeneration in development and disease. *Annu Rev Neurosci* 28:127–156.
4. Birse SC, Bittner GD (1976) Regeneration of giant axons in earthworms. *Brain Res* 113: 575–581.
5. Hoy RR, Bittner GD, Kennedy D (1967) Regeneration in crustacean motoneurons: Evidence for axonal fusion. *Science* 156:251–252.
6. Deriemer SA, Elliott EJ, Macagno ER, Muller KJ (1983) Morphological evidence that regenerating axons can fuse with severed axon segments. *Brain Res* 272:157–161.
7. Macagno ER, Muller KJ, DeRiemer SA (1985) Regeneration of axons and synaptic connections by touch sensory neurons in the leech central nervous system. *J Neurosci* 5:2510–2521.
8. Bedi SS, Glanzman DL (2001) Axonal rejoining inhibits injury-induced long-term changes in Aplysia sensory neurons in vitro. *J Neurosci* 21:9667–9677.
9. Ghosh-Roy A, Wu Z, Goncharov A, Jin Y, Chisholm AD (2010) Calcium and cyclic AMP promote axonal regeneration in Caenorhabditis elegans and require DLK-1 kinase. *J Neurosci* 30:3175–3183.
10. Ghosh-Roy A, Chisholm AD (2010) Caenorhabditis elegans: A new model organism for studies of axon regeneration. *Dev Dyn* 239:1460–1464.
11. Chen L, et al. (2011) Axon regeneration pathways identified by systematic genetic screening in C. elegans. *Neuron* 71:1043–1057.
12. Nix P, et al. (2014) Axon regeneration genes identified by RNAi screening in C. elegans. *J Neurosci* 34:629–645.
13. Hammarlund M, Jin Y (2014) Axon regeneration in C. elegans. *Curr Opin Neurobiol* 27:199–207.
14. Neumann B, Nguyen KC, Hall DH, Ben-Yakar A, Hilliard MA (2011) Axonal regeneration proceeds through specific axonal fusion in transected C. elegans neurons. *Dev Dyn* 240:1365–1372.
15. Neumann B, et al. (2015) EFF-1-mediated regenerative axonal fusion requires components of the apoptotic pathway. *Nature* 517:219–222.
16. Yanik MF, et al. (2004) Neurosurgery: Functional regeneration after laser axotomy. *Nature* 432:822.
17. Bounoutas A, Chalfie M (2007) Touch sensitivity in Caenorhabditis elegans. *Pflugers Arch* 454:691–702.
18. Fang-Yen C, Gabel CV, Samuel AD, Bargmann CI, Avery L (2012) Laser microsurgery in Caenorhabditis elegans. *Methods Cell Biol* 107:177–206.
19. Benninger RK, Piston DW (2013) Two-photon excitation microscopy for the study of living cells and tissues. *Curr Protoc Cell Biol* Chapter 4:Unit 4 11.
20. Wu Z, et al. (2007) Caenorhabditis elegans neuronal regeneration is influenced by life stage, ep a Howard Hughes Medical Institute International Early Career Scientist Award in signaling, and synaptic branching. *Proc Natl Acad Sci USA* 104:15132–15137.
21. Williams W, Nix P, Bastiani M (2011) Constructing a low-budget laser axotomy system to study axon regeneration in C. elegans. *J Vis Exp* 3331.
22. Byrne AB, Edwards TJ, Hammarlund M (2011) In vivo laser axotomy in C. elegans. *J Vis Exp* 2707.
23. Hobert O, Johnston RJ, Jr, Chang S (2002) Left-right asymmetry in the nervous system: The Caenorhabditis elegans model. *Nat Rev Neurosci* 3:629–640.
24. Chalfie M, et al. (1985) The neural circuit for touch sensitivity in Caenorhabditis elegans. *J Neurosci* 5:956–964.
25. Ghosh-Roy A, Goncharov A, Jin Y, Chisholm AD (2012) Kinesin-13 and tubulin posttranslational modifications regulate microtubule growth in axon regeneration. *Dev Cell* 23:716–728.
26. Kim E, Sun L, Gabel CV, Fang-Yen C (2013) Long-term imaging of Caenorhabditis elegans using nanoparticle-mediated immobilization. *PLoS One* 8:e53419.
27. Guo SX, et al. (2008) Femtosecond laser nanoaxotomy lab-on-a-chip for in vivo nerve regeneration studies. *Nat Methods* 5:531–533.
28. Mohler WA, et al. (2002) The type I membrane protein EFF-1 is essential for developmental cell fusion. *Dev Cell* 2:355–362.
29. Zou Y, et al. (2013) Developmental decline in neuronal regeneration by the progressive change of two intrinsic timers. *Science* 340:372–376.
30. Chen L, et al. (2015) Axon injury triggers EFA-6 mediated destabilization of axonal microtubules via TACC and doublecortin like kinase. *Elife,* 4.
31. Reinhart BJ, et al. (2000) The 21-nucleotide let-7 RNA regulates developmental timing in Caenorhabditis elegans. *Nature* 403:901–906.
32. Slack FJ, et al. (2000) The lin-41 RBCC gene acts in the C. elegans heterochronic pathway between the let-7 regulatory RNA and the LIN-29 transcription factor. *Mol Cell* 5:659–669.
33. Bagga S, et al. (2005) Regulation by let-7 and lin-4 miRNAs results in target mRNA degradation. *Cell* 122:553–563.
34. Pfaffl MW (2001) A new mathematical model for relative quantification in real-time RT-PCR. *Nucleic Acids Res* 29:e45.
35. Vella MC, Choi EY, Lin SY, Reinert K, Slack FJ (2004) The C. elegans microRNA let-7 binds to imperfect let-7 complementary sites from the lin-41 3'UTR. *Genes Dev* 18: 132–137.
36. Byrne AB, et al. (2014) Insulin/IGF1 signaling inhibits age-dependent axon regeneration. *Neuron* 81:561–573.
37. Gabel CV, Antoine F, Chuang CF, Samuel AD, Chang C (2008) Distinct cellular and molecular mechanisms mediate initial axon development and adult-stage axon regeneration in C. elegans. *Development* 135:1129–1136.
38. Verdú E, Ceballos D, Vilches JJ, Navarro X (2000) Influence of aging on peripheral nerve function and regeneration. *J Peripher Nerv Syst* 5:191–208.
39. Geoffroy CG, Hilton BJ, Tetzlaff W, Zheng B (2016) Evidence for an age-dependent decline in axon regeneration in the adult mammalian central nervous system. *Cell Rep* 15:238–246.
40. Luo S, Schaefer AM, Dour S, Nonet ML (2014) The conserved LIM domain-containing focal adhesion protein ZYX-1 regulates synapse maintenance in Caenorhabditis elegans. *Development* 141:3922–3933.
41. Mondal S, Ahlawat S, Rau K, Venkataraman V, Koushika SP (2011) Imaging in vivo neuronal transport in genetic model organisms using microfluidic devices. *Traffic* 12: 372–385.
42. Goodman MB (2006) Mechanosensation. *Wormbook* 1–14.
43. White JG, Southgate E, Thomson JN, Brenner S (1986) The structure of the nervous system of the nematode Caenorhabditis elegans. *Philos Trans R Soc Lond B Biol Sci* 314:1–340.
44. Qiu J, et al. (2002) Spinal axon regeneration induced by elevation of cyclic AMP. *Neuron* 34:895–903.
45. Park KK, et al. (2008) Promoting axon regeneration in the adult CNS by modulation of the PTEN/mTOR pathway. *Science* 322:963–966.
46. Hellal F, et al. (2011) Microtubule stabilization reduces scarring and causes axon regeneration after spinal cord injury. *Science* 331:928–931.
47. Ambros V, Horvitz HR (1984) Heterochronic mutants of the nematode Caenorhabditis elegans. *Science* 226:409–416.
48. Kravtsov V, Oren-Suissa M, Podbilewicz B (2017) The fusogen AFF-1 can rejuvenate the regenerative potential of adult dendritic trees by self-fusion. *Development* 144: 2364–2374.
49. Brenner S (1974) The genetics of Caenorhabditis elegans. *Genetics* 77:71–94.
50. Chalfie M, Hart AC, Rankin CH, Goodman MB (2014) Assaying mechanosensation. *WormBook*, 10.1895/wormbook.1.172.1.
51. Hobert O, Moerman DG, Clark KA, Beckerle MC, Ruvkun G (1999) A conserved LIM protein that affects muscular adherens junction integrity and mechanosensory function in Caenorhabditis elegans. *J Cell Biol* 144:45–57.
52. Chalfie M, Sulston J (1981) Developmental genetics of the mechanosensory neurons of Caenorhabditis elegans. *Dev Biol* 82:358–370.
53. Bracht J, Hunter S, Eachus R, Weeks P, Pasquinelli AE (2004) Trans-splicing and polyadenylation of let-7 microRNA primary transcripts. *RNA* 10:1586–1594.
54. Broughton JP, Lovci MT, Huang JL, Yeo GW, Pasquinelli AE (2016) Pairing beyond the seed supports microRNA targeting specificity. *Mol Cell* 64:320–333.
55. Kirszenblat L, Neumann B, Coakley S, Hilliard MA (2013) A dominant mutation in mec-7/β-tubulin affects axon development and regeneration in Caenorhabditis elegans neurons. *Mol Biol Cell* 24:285–296.
56. Sutphin GL, Kaeberlein M (2009) Measuring Caenorhabditis elegans life span on solid media. *J Vis Exp* 1152.